JOURNAL OF CATALYSIS 147, 484–493 (1994)

Synthesis and Characterization of ZSM-22 Zeolites and Their Catalytic Behavior in 1-Butene Isomerization Reactions

Mark W. Simon,* Steven L. Suib,*,†,[1] and Chi-Lin O'Young‡,[1]

*U-60, Department of Chemistry, University of Connecticut, Storrs, Connecticut 06269-3060; †Department of Chemical Engineering and Institute of Material Sciences, University of Connecticut, Storrs, Connecticut 06269-3060; and ‡Texaco, Inc., P.O. Box 509, Beacon, New York 12508

Received September 20, 1993; revised January 14, 1994

ZSM-22 zeolites, having a Si/Al ratio of 45, have been synthesized by sol–gel methods using 1,6-diaminohexane as a templating agent. The structures of these materials have been characterized by X-ray diffraction, transmission electron microscopy and electron diffraction, scanning electron microscopy, and adsorption techniques. Based on these analyses, these materials are determined to be of the Theta-1 structure type. Titration with pyridine base shows that these catalysts have a Brønsted to Lewis ratio of 7.0. Temperature programmed desorption experiments with NH_3 show that both strong and weak acid sites are present in this material and that the ratio of strong acid sites to weak acid sites is 1.1. From this information a total of 0.96 H^+ sites/u.c. has been calculated for this material, suggesting that these catalysts have relatively low acidity. The unique unidirectional pore structure and accompanying high Si/Al ratio of ZSM-22 provide for a potentially useful isomerization catalyst. These materials are used in this study for the isomerization of 1-butene, where shape selectivity is believed to be important in this first order reaction. Other kinetic information is obtained through deactivation studies and from studies of the effect of flow rates and temperature on conversion, selectivity, and yields of isobutylene. Yields and selectivities of 39.5 and 89%, respectively, have been obtained with this catalyst system. © 1994 Academic Press, Inc.

I. INTRODUCTION

The production of isobutylene (i-C_4H_8) by methods other than thermal cracking has been of considerable interest recently. Isobutylene is an important feed stock in the production of isoprene and methacrylic acid which are used as additives in the polymer industry (1). Isobutylene is also a raw material for the production of methyl *tert*-butyl ether (MTBE), an oxygenated fuel additive having a high octane number.

The release of volatile gasoline fractions like n-butanes and butenes into the atmosphere during pumping and transfer of gasoline has prompted oil producers to develop new hydrocarbon conversion reactions of these fractions into less volatile components. The release of volatile fractions into the atmosphere is detrimental to the ozone layer. For this reason, research in butene isomerization reactions to isobutylene has been of great significance recently. The 1990 U.S. clean air act amendments specify that gasoline containing a minimum of 2.7 wt.% oxygen must be sold in 39 CO nonattainment cities in the U.S. This is resulting in an increased demand for MTBE (2), and thus an increased demand for isobutylene production.

ZSM-22 has the Theta-1 structure type and consists of single rings and a unidirectional and one-dimensional 10-membered tetrahedral ring channel system (3, 4). This microporous material lacks channel intersections and associated pore volumes, suggesting that this system may have structurally specific properties. Recently, Thomas has suggested, based on theoretical modeling, that 10 membered ring zeolites would be useful in the transformation of n-butenes to isobutylene (5). Theta-1 zeolites have been compared to other medium-pore zeolites such as ZSM-5, ZSM-11, and ferrierite zeolites based on their high silica content and 10-T-ring channels, although these structures have different specific topologies from ZSM-22 (6). Borade *et al.* have recently reported the synthesis, characterization, and acidity of ZSM-22 zeolites (7). Besides ZSM-22, several other high silica zeolites having the Theta-1 structure type have been synthesized. These isotypic framework structures include ISI-1 (8, 9), KZ-2 (10), and NU-10 (11, 12).

Methanol to hydrocarbon conversions have been applied to KZ-2 zeolites resulting in high yields of aromatics (10, 13). Similar results were achieved over ZSM-5 and NU-10 (14) zeolites. Theta-1 type zeolites have also been used in xylene isomerization (15), alkylation of toluene with methanol to p-xylene (16–18), and in the conversion of dimethyl ether and monofunctional alcohols to lower olefins (12). ZSM-22 zeolites have been applied in the catalytic dewaxing of petroleum feed stocks (18). We have recently reported that n-butanes and butenes isomerize

[1] To whom correspondence should be addressed.

0021-9517/94 $6.00
Copyright © 1994 by Academic Press, Inc.
All rights of reproduction in any form reserved.

to isobutylene over isomorphously substituted B-ZSM-5 zeolites (19).

This paper focuses on the application of ZSM-22 zeolites to n-C_4H_8 isomerization reactions, the kinetics of reaction, and deactivation and regeneration of these catalysts. Supporting characterization work from X-ray diffraction (XRD), Fourier transform infrared spectroscopy (FTIR), temperature programmed desorption (TPD) studies, transmission electron microscopy (TEM), and gravimetric desorption techniques is also mentioned. Elemental analysis was performed by inductively coupled plasma (ICP).

II. EXPERIMENTAL

A. Synthesis

1. Sol–gel formation. A sol–gel was formed by adding, with vigorous stirring, a solution of $Al_2(SO_4)_3 \cdot 18H_2O$ containing KOH and 1,6-diaminohexane as a templating agent to a sol of colloidal silica. The gel was obtained according to a recipe for the synthesis of ZSM-22 from Ref. (20). The resulting gel, having a molar composition of 110 SiO_2 : Al_2O_3 : 19 K_2O : 33 $NH_2(CH_2)_6NH_2$: 4384 H_2O, was transferred into a 450-cm^3 Teflon-lined, stainless-steel autoclave. The gel was stirred at approximately 70 rpm in a furnace at 165°C for 48 h. Following heating, the autoclave was quenched in cold water and the white crystals were recovered by filtering and washing with deionized distilled water (DDW).

2. Calcination, ion-exchange, and deammoniation. The sample was calcined in air by slowly increasing the temperature 3°C/min from 25 to 550°C. The temperature was held at 550°C for 12 h.

The resulting K^+/ZSM-22 zeolite was ion-exchanged two times with a 1.0 M solution of NH_4NO_3 in a magnetically stirred round bottom flask at 80°C for 12 h. About 100 mL of ammonium nitrate was used per g of zeolite. The zeolite was filtered and washed three times with 5 mL of DDW.

The resulting NH_4^+/ZSM-22 zeolite was deammoniated by heating to 550°C with a heating rate of 3°C/min in flowing Ar (30 cm^3/min). The temperature was held at 550°C for 8 h.

B. Characterization

XRD experiments were carried out on a Scintag Model PDS 2000 diffractometer. Cu$K\alpha$ radiation was used as the X-ray source. Samples were run at a step time of 2 s and a step size of 0.030°. Peak locations were normalized by using quartz as an internal standard.

TEM experiments were carried out on an EM-420 Phillips analytical electron microscope having a resolution of 2 Å. Secondary electron imaging of single crystals and agglomerates were obtained. TEM micrographs and diffraction patterns were also obtained.

FTIR spectroscopy experiments were performed on a Mattson Galaxy spectrometer with a home-built *in situ* IR cell. A scan resolution of 2 cm^{-1} was used for the analysis. Exactly 15 mg of H^+/ZSM-22 was pressed into a self-supporting pellet, placed in the IR cell, and treated in a manner previously described (21).

Acidity was measured by quantitative analysis (at ambient temperature) of sorbed pyridine on the zeolite as described elsewhere (19, 21). The peak at 1545 cm^{-1} was integrated to determine the Brønsted acidity. This peak was compared to the peak at 1460 cm^{-1}, which corresponds to Lewis acidity.

For framework vibrational frequencies, 0.5 mg of sample was mixed with 50 mg of KBr (spectroscopic grade), ground into a fine powder, and pressed into a pellet. The infrared spectrum was taken from 4000 to 500 cm^{-1}.

TPD experiments were carried out on a TPD apparatus previously described (22). A thermal conductivity detector was used on a Varian Series 1400 gas chromatograph. Ammonia was adsorbed at 100°C for 100 min on a thoroughly dehydrated zeolite. A heating rate of 15°C/min was used during desorption. Details on this procedure can be found elsewhere (19).

Surface areas were measured by adsorption of N_2 at 77 K on a Cahn microbalance by a gravimetric technique. The BET equation was used to determine surface area. The BET equation can be applied to systems in which the pore size is >4.0 Å. N_2 adsorption experiments are frequently applied to zeolites to determine surface area. Sorption pressures ranged from 0.003 Torr to about 300 Torr at 77 K. Desorption was carried out between 25 and 395°C with a heating rate of 5°C/min and an outgassing pressure of 1×10^{-5} Torr.

A Perkin–Elmer P-40 inductively coupled plasma atomic emission spectrophotometer (ICP-AES) was used for elemental analyses. The samples were dissolved in acids, heated by microwave, and digested in a Teflon-lined bomb.

C. Catalysis

1. Definition of terms. Data was analyzed by using the material balance:

$$\text{INPUT} + \text{RATE} = \text{OUTPUT} + \text{ACCUMULATION} \quad [1]$$

Rates of oligomerization (>C_4 by-products) were determined based on the material balance. At steady state the accumulation term approaches zero, and nearly all oligomers generated are present in the gas phase, not on the catalyst. Under non-steady state conditions, however,

rates of oligomerization include gas phase oligomers as well as coked species on the catalyst. Coking on the catalyst is represented by the accumulation term in the material balance. Input feed rates are set based on the flow rate, the partial pressure of the feed gas, and the weight of the catalyst. The generation term represents the loss of reactant, determined chromatographically. The output term of the material balance represents unreacted starting material, measured chromatographically.

Products and reactants from C_1 to C_4 were separated chromatographically and areas were calibrated using FID response factors. Flow analyses and reaction order experiments were done following 20 h time on stream, when near steady state conditions are reached. This is done in order to simplify Eq. [2] and to avoid effects of deactivation. Order of reaction experiments were run at conversions <5% in order to apply differential rate equations. In this case, Eq. [2], based on the ideal gas law, is applied:

$$-d[n\text{-}C_4H_8]/dt = (PQ_o/RT_o)y_i/W, \quad [2]$$

where P is total pressure (1 atm), Q_o is flow rate in cm^3/min (ambient), R is the ideal gas constant (82.057×10^{-6} cm^3-atm/μmol K), T_o is 298 K, y_i is the mole fraction of i, and W is weight of catalyst in g. Rate has units of μmol/min · g. The gas compressibility factor, Z, for butene was calculated to be approximately 1, thus not affecting the number of moles of gas phase butene determined by volumetric flow. Gas liquefaction of butene is also not a factor at operating pressures.

Conversion, X_A, is defined as the carbon molar conversion percentage of each feed and is determined by Eq. [3]

$$X_A = (c_{IN} - c_{OUT})/c_{IN} \times 100\%, \quad [3]$$

where c_{IN} is the concentration of 1-C_4H_8 flowing into the reactor and c_{OUT} is the Σ 1-C_4H_8, c-2-C_4H_8, t-2-C_4H_8 concentrations measured at the effluent of the reactor. Note that c-2-C_4H_8 and t-2-C_4H_8 are considered as unreacted starting material because at reaction temperatures an equilibrium is established between 1-butene and the 2-butene isomers. Yields and selectivities discussed in this paper refer to those of isobutylene, where selectivity is defined as yield/conversion.

2. Catalytic experiments. Specified masses of catalyst were weighed on a Mettler balance to ±0.001 g and loaded into the microreactor. A description of the reactor and catalyst bed preparations can be found elsewhere (19). The catalyst was activated at 550°C under an argon purge (30 cm^3/min). The temperature was elevated at 50°C intervals per hour until final treatment temperatures were reached.

A Carle 1000 gas chromatograph (GC) with a flame ionization detector (FID) was used for analysis. Operational conditions for chromatographic separations, GC calibration procedures, and gas mixing techniques for feed gases have been described previously (19).

Flow rates of treatment gases and reaction mixtures were controlled with fine metering valves and measured by bubble meters under ambient conditions (1 atm, 298 K). A diagram of the reactor and flow system is shown in Fig. 1.

III. RESULTS

A. Characterization

Secondary electron imaging at 12,000 magnification showed uniform needle-like crystals. The crystals were found to have a length of 1–2 μm and a width of about 100 Å or less.

Unit cell parameters were obtained by direct measurement from TEM micrographs. These values compare well with unit cell parameters determined by indexing 13 calibrated and refined lines of the X-ray diffraction pattern. d-Spacings were measured for five other Miller indices having well defined and intense electron diffraction dot patterns. Systematic absences were observed for the [$h0l$] reflections for which $l \neq 2n$.

The X-ray diffraction pattern of the K^+ form of ZSM-22 zeolite, shown in Fig. 2, agrees well with that reported in the literature for H^+/ZSM-22 (20). A significant decrease in peak intensities at high d-spacings was observed in our analysis of K^+/ZSM-22 compared to H^+/ZSM-22 reported in Ref. (20). This has been attributed to the presence of different cations in the two materials.

Unit cell parameters obtained for the K^+/ZSM-22 zeolite were $a = 13.86 \pm 0.03$ Å, $b = 17.41 \pm 0.04$ Å, and $c = 5.05 \pm 0.01$ Å. The unit cell volume was calculated to be 1217 Å^3.

Five sharp bands in the infrared spectrum are observed between 1500 and 400 cm^{-1}. Beyond 1500 cm^{-1}, two very broad bands corresponding to surface hydroxyl groups and strongly bonded chemisorbed water are detected between 3800 and 3200 cm^{-1}. A characteristic shoulder at 1220 cm^{-1} is also apparent.

The FTIR spectrum of pyridine adsorbed on H^+/ZSM-22 is shown in Fig. 3. From these data a Brønsted-to-Lewis ratio of 7.0 was determined.

ZSM-22 zeolite follows Type 1 adsorption behavior, typical for microporous materials, particularly zeolites. A surface area of 145.7 m^2/g was obtained for the calcined H^+/ZSM-22 zeolite. The contribution from meso- and macroporosity amounted to 9.09 m^2/g. Nearly 95% of the porosity in these materials results from the microporosity of the sample. This was determined by using a T-plot, which is a plot of volume of N_2 adsorbed versus film

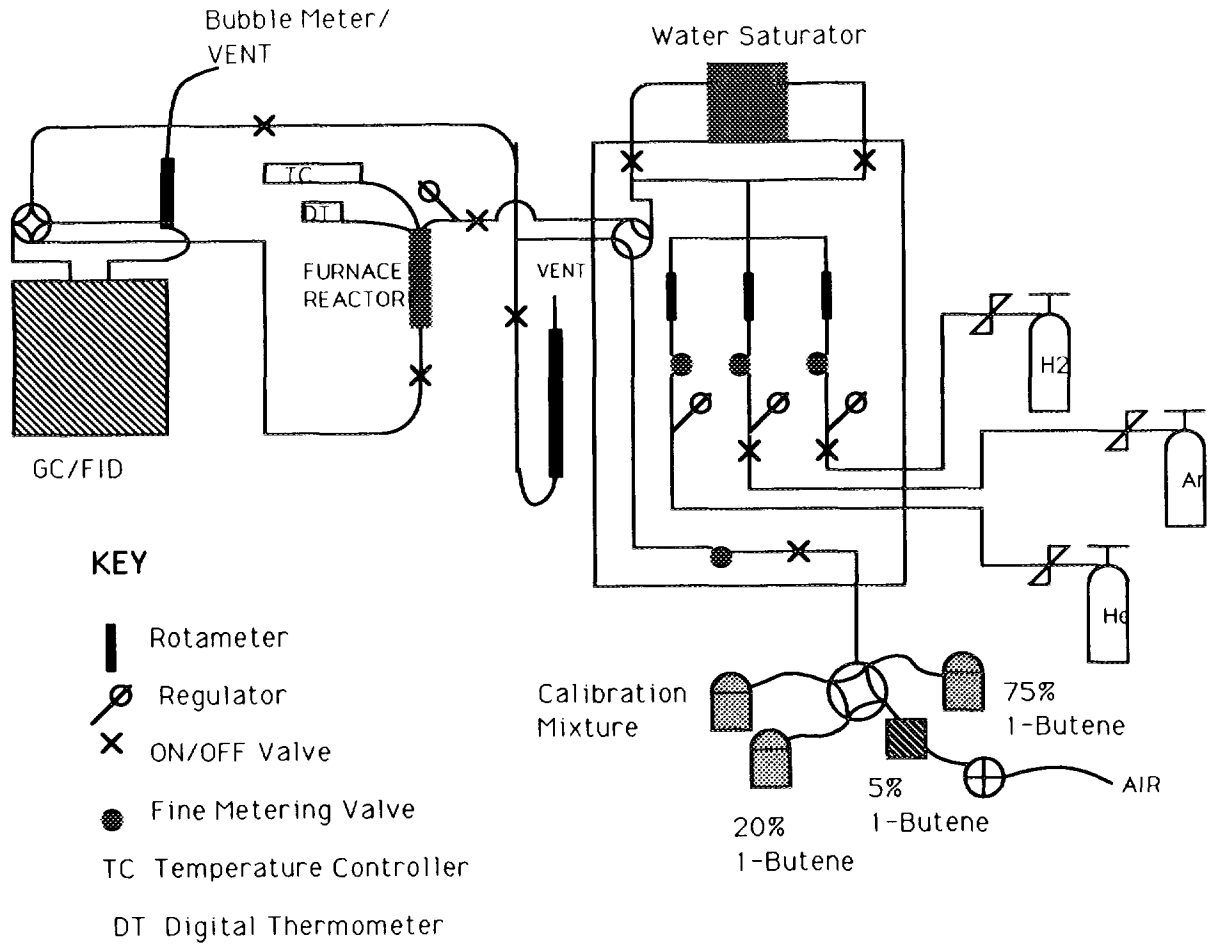

FIG. 1. Reactor and flow system.

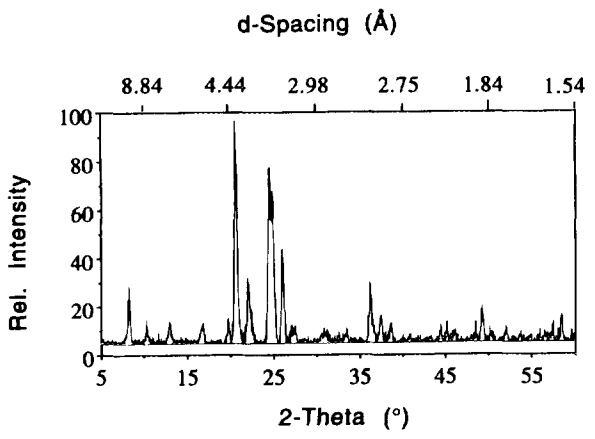

FIG. 2. X-ray powder diffraction of hydrated K^+/ZSM-22 zeolite, calcined at 500°C in N_2 for 8 h then at 550°C in 20% O_2/Ar for 8 h. Step size = 0.030°; scan from 5 to 60° 2-Theta.

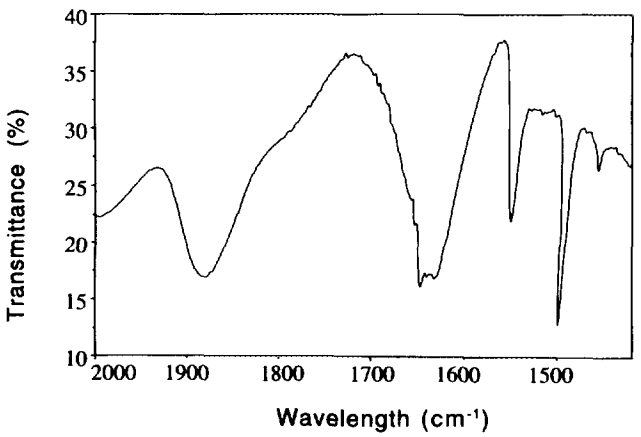

FIG. 3. Fourier transform infrared spectrum of chemisorbed pyridine on ZSM-22 zeolite. Dehydration of zeolite at 550°C, followed by room-temperature adsorption of pyridine, and then removal of physisorbed pyridine for 8 h at 150°C and 1×10^{-5} Torr.

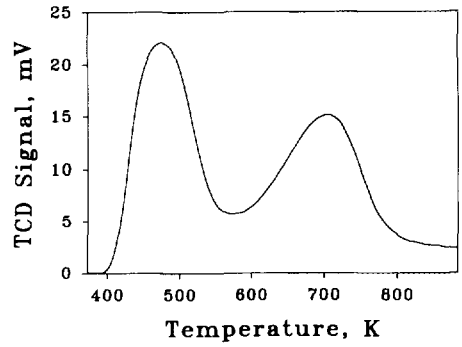

FIG. 4. Temperature programmed desorption of NH_3 from 100 to 690°C. Adsorption of 100% NH_3 for 30 min at 100°C on 40 mg of dehydrated zeolite for He purge followed by 40 min, then TPD in Ar (30 cm^3/min) β = 15°C/min.

thickness (Å). The film thickness is determined by monolayer coverage on a nonporous material identical to that under study. An exact pore size distribution was difficult to obtain for these materials, and thus surface areas were used as a means of comparing these materials to those reported in the literature, although pore volumes are more characteristic of zeolites than surface areas.

The TPD spectrum of H^+/ZSM-22 zeolite, shown in Fig. 4, reveals two peaks corresponding to two types of acid sites, of different strengths. The two TPD peaks were integrated and amounts of adsorbed ammonia are reported in μmol/g. The peak located at T_M = 201°C had an area equivalent to 332 μmol of adsorbed NH_3/g of catalyst, while the peak at T_M = 332°C had an area equivalent to 341 μmol of adsorbed NH_3/g of catalyst. The sum of these values is equivalent to a total adsorption of 0.96 NH_3 molecules per unit cell. The ratio of strong-to-weak adsorption sites was 1.1.

ICP results show a Si/Al ratio of 45 : 1. This is consistent with Theta-1 materials (20).

B. Catalysis

Kinetic studies on the transformation of *n*-butenes into isobutylene were first done by optimizing reaction conditions. Temperature was studied in a range between 300 and 480°C. Higher temperatures caused high conversion and, as a result, low selectivity. Increased yields of higher olefins were also observed at higher temperatures. Faster rates of deactivation were observed at elevated temperatures. The optimized reaction temperature in terms of yield and selectivity was found to be 420°C. Rates of deactivation were reduced to less than 25% (total conversion) at 420°C over a 20 h period. Conversions, yields, selectivities, and oligomer formation are reported in Table 1 for some of the temperatures studied. Maximum theoretical yields based on thermodynamic calculations are shown in the last column of Table 1.

TABLE 1

Catalytic Activity for *n*-C_4H_8 Isomerization over ZSM-22 Zeolite as a Function of Temperature

Temperature (°C)	Conversion (%)	Selectivity (%)	Oligomer (mol%)	Actual yield (mol%)	Theoretical yield[a] (mol%)
300	34.8	67.3	5.0	23.5	47.3
340	33.9	64.3	6.3	21.8	43.8
420	59.6	54.4	9.8	33.6	39.7
460	62.0	54.2	11.9	32.5	37.9
480	66.9	41.3	18.9	27.7	37.4

Note. 20% *n*-C_4H_8/Ar, 20 cm^3/min, 1 atm, W = 120 mg, time on stream > 15 h.

[a] Maximum yield of isobutylene based on thermodynamic equilibrium calculations.

In flow analyses, ZSM-22 zeolite was tested at flow rates between 3.5 and 100 cm^3/min, which correspond to weight hour space velocities (WHSV) between 4.6 and 13.8 h^{-1} for 120 mg of catalyst and a 20% feed of 1-C_4H_8. Flow experiments were done at 420°C after 18 h of reaction, where yields are optimized and near steady state conditions are achieved. Time on stream data will be discussed later. Conversions increased from 47% at 100 cm^3/min to 74% at 3.5 cm^3/min. Increasing flow rates resulted in higher yields of isobutylene. Yields of 31% were observed at 20 cm^3/min, while at 100 cm^3/min yields of 40% were achieved. Selectivities decreased from 85% at 100 cm^3/min to 27% at 3.5 cm^3/min. Oligomer formation was reduced to less than 1% at 100 cm^3/min. Conversions, selectivities, and yields are plotted as a function of space velocity in Fig. 5 and a complete list of these results is shown in Table 2.

Time on stream analyses up to 20 h show that at 420°C with 60 mg of catalyst and a flow rate of 30 cm^3/min that slow deactivation occurs with rates decreasing from 124

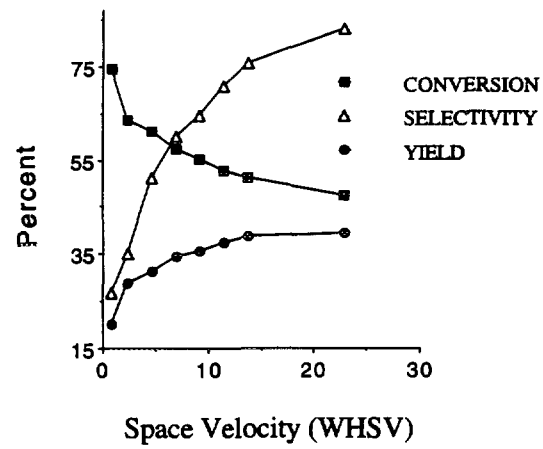

FIG. 5. Percent conversion, yield, and selectivity vs flow rate at 420°C, 120 mg ZSM-22, 20% 1-C_2H_8 reactant.

TABLE 2

Catalytic Activity for n-C_4H_8 Isomerization over ZSM-22 Zeolite as a Function of Flow Rate

Flow (cm^3/min)	Conversion (%)	Yield (mol%)	Selectivity (%)	Oligomer (mol%)
3.5	74.4	20.1	26.8	19.6
10	63.6	28.9	45.4	11.6
20	61.1	31.3	51.2	10.9
30	57.3	34.5	60.1	9.7
40	55.2	35.6	64.5	8.2
50	52.6	37.3	70.8	6.4
60	51.1	38.6	75.6	3.7
100	47.4	39.5	84.8	0.98

Note. 20% n-C_4H_8/Ar, 420°C, 1 atm, W = 120 mg.

μmol/min · g to 92 μmol/min · g. This results in an average differential deactivation rate of 3.1 μmol/h · g for the first 7.5 h, and a much slower deactivation rate of 0.6 μmol/h · g for longer times on stream. These results are shown in Fig. 6.

Figure 7 shows a typical distribution of reaction by-products as a function of time on stream. The conversion range of these curves is between 30 and 40% and yields of isobutylene are near 27%. All reaction by-products decrease with increasing time on stream. Propylene is observed to be the major reaction by-product. Some hydrogenation of butenes to butanes is also observed. Formation of oligomers is also observed to decrease from 6 to 2% with decreasing time on stream.

Following 20 h of reaction at 420°C with 20% 1-C_4H_8, the catalyst was removed from the reactor and weighed. Amount of coke formed on the catalyst was determined by differences in weight, before and after reaction. The sample mass increased by 4.2%, which is equivalent to the wt.% of coke on the catalyst formed under these conditions.

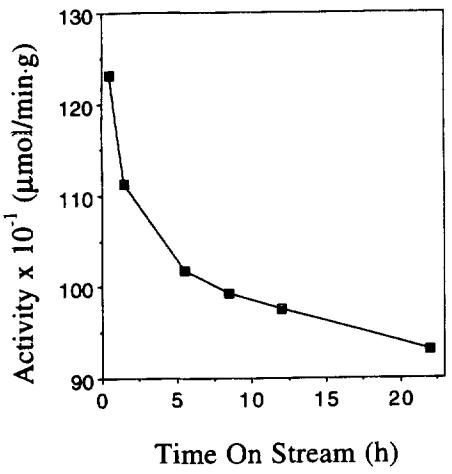

FIG. 6. Activity (μmol/min · g × 10^{-1}) vs time on stream (h) at 420°C, 20 cm^3/min, 60 mg ZSM-22, 20% 1-C_4H_8 reactant.

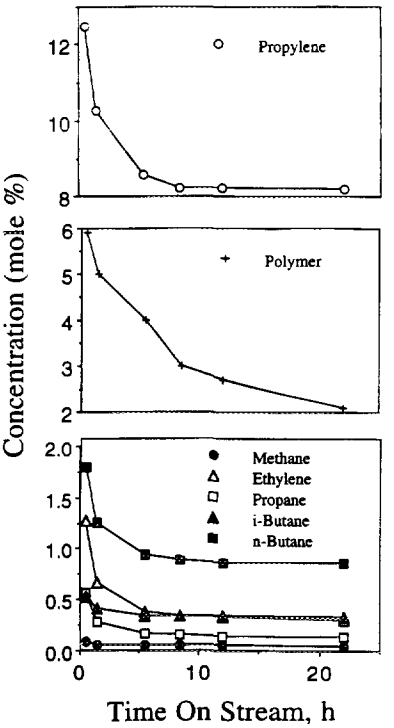

FIG. 7. Distribution of products: mol% vs time on stream (h) at 420°C, 20 cm^3/min, 120 mg catalyst, 20% 1-C_4H_8 reactant.

Deactivation data at 420°C and a space velocity of 4.58 h^{-1} can be found in Table 3. These data show conversions, yields, selectivities, and oligomer formation during the first 5.5 h time on stream, when deactivation is most severe. Table 3 shows an increase in yields with increasing time on stream. High conversions (70%) result in rapid rates of deactivation, causing the rates of isobutylene

TABLE 3

Catalytic Results for n-C_4H_8 Isomerization over ZSM-22 Zeolite as a Function of Time on Stream at High Conversions

TOS (min)	Conversion (%)	Yield (mol%)	Selectivity (%)	Oligomer (mol%)
10	72.5	21.6	29.8	11.6
20	71.6	22.6	31.6	10.8
30	70.8	23.8	33.6	9.8
50	70.1	24.1	34.4	9.8
150	67.7	26.4	39.0	7.5
230	65.9	27.9	42.3	4.9
270	64.5	28.0	43.3	3.5
320	63.4	29.2	46.0	2.6

Note. 20% n-C_4H_8/Ar, 20 cm^3/min, 420°C, 1 atm, W = 120 mg.

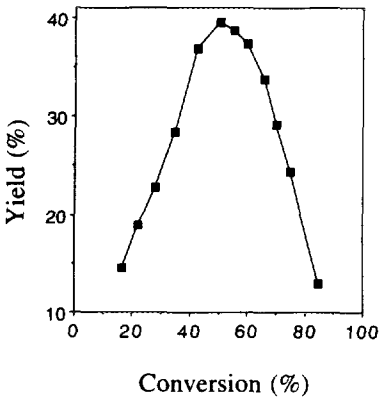

FIG. 8. Conversion (%) vs yield (%) over ZSM-22 catalyst at 420°C, after reaching equilibrium.

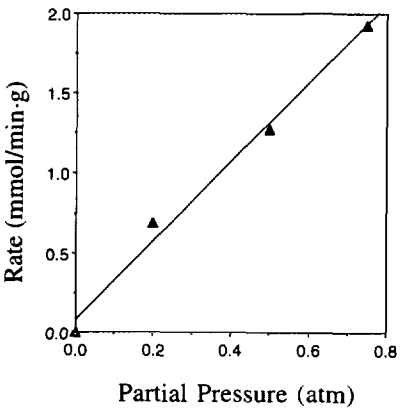

FIG. 9. Rate of isobutylene formation (mmol/min · g) vs partial pressure (atm) of 1-C_4H_8 at 420°C and 30 cm^3/min.

production to increase. At high conversions yields of C_3H_6 begin to dominate. Deactivation continues to occur until lower conversions are reached and yields of isobutylene are optimized. It was also observed that lower conversions (<40%) resulted in low rates of deactivation and decreased yields of isobutylene. Optimum yields of isobutylene are highly dependent on the extent of conversion. Due to this strong dependence of conversion on yield, the optimum conversion range was determined.

Optimal yields of isobutylene are observed at conversions near 47%, as shown in Fig. 8. Low conversions (and yields) were obtained by reducing the catalyst mass and increasing the flow rates (increasing the WHSV). High conversions were achieved by decreasing the space velocity. A typical product distribution at optimized conditions (T = 420°C, 13.6 h^{-1}, X_A = 47%) is shown in Table 4.

Studies of the rate of reaction (mmol/min · g) vs partial pressure (atm) of 1-butene are shown in Fig. 9. A linear increase in rate with partial pressure is observed. A 5% conversion was used to minimize the rate of deactivation. In this experiment 20 mg of catalyst, a flow rate of 60 cm^3/min, and a temperature of 420°C were used to achieve low conversions.

TABLE 4

A Typical Product Distribution for n-C_4H_8 Isomerization over ZSM-22 Zeolite at Optimum Operating Conditions

Product	Rate (μmol/min · g)	Concentration (mol%)
Methane	0.0	0.0
Ethylene	16.9	0.27
Propane	8.21	0.13
Propylene	299	4.81
i-Butane	4.72	0.08
n-Butane	110	1.77
i-Butylene	2450	39.4
C5-C9	136	2.20

Note. A 20% n-C_4H_8/Ar, 100 cm^3/min, 1 atm, W = 120 mg, 22.9 WHSV.

IV. DISCUSSION

The X-ray diffraction pattern shown in Fig. 2 is in excellent agreement with the Theta-1 structure type (7, 20). Values of unit cell parameters and volumes of unit cells are consistent with literature reports (3, 4, 6, 12).

It has been reported that impurities of α-crisobalite are often detected in the XRD pattern of synthetic ZSM-22 (3, 12). Two peaks are associated with this impurity; the first at d = 4.16 Å and the second at d = 3.81 Å. The peak at 3.81 Å in Fig. 2 corresponds to α-crisobalite; however, this impurity is in small amounts and the peak at 4.16 Å is not apparent. There is no evidence of such material in SEM or TEM experiments. Secondary electron imaging clearly shows needle-like crystals, consistent with ZSM-22, (both in size and shape) to previous reports (7, 20). The systematic absences in the [$h0l$] reflections observed in our materials are consistent with $Cmc2_1$ symmetry, previously reported for ZSM-22 zeolites (6). All structural data agree with the Theta-1 structure type. We have called this material ZSM-22 because it was obtained using the synthetic recipe for ZSM-22 found in Ref. (20). Recently, other synthetic procedures have also been studied (7).

Framework vibrations observed in the infrared are characteristic of Theta-1 zeolites. Both Si–O stretching (ν) and deformation (δ) vibrations are observed in these materials and are consistent with those reported for other Theta-1 type zeolites (11).

Based on pyridine chemisorption studies, shown in Fig. 3, this material exhibits high Brønsted acidity. Acidity

measurements by means of NH_3 desorption, as in Fig. 4, show two sites of different acid strength. Earlier studies by Ernst *et al.* showed that the H^+ form of ZSM-22 contains surface hydroxyl groups which are identical to those found in H-ZSM-5 (20). In earlier work, boron was isomorphously substituted into the ZSM-11 framework in order to reduce acidity (23). Strong acidity results in dimerization of olefins which can then crack on acid sites. TPD data suggest that this material has relatively low acidity. Acidity measurements obtained in this study are consistent with previous reports on ZSM-22 zeolites (7).

These zeolites have a relatively low surface area compared to most zeolites, suggesting that ZSM-22 has a low void volume. ZSM-22 zeolites lack void "cage" volumes of ZSM-5 associated with the two-dimensional channel system. From our analyses it has been shown that the surface areas of Theta-1 zeolites can be as much as half the surface areas of other 10-membered ring zeolites, such as ferrierite. This might be expected because Theta-1 zeolites have one-dimensional, unidirectional channels (4.7 × 5.5 Å) with only a 10-T-ring system, while ferrierite zeolites have two-dimensional channels and both an 8 and 10-T-ring system. The surface areas of ZSM-22 materials compare well with those reported for other Theta-1 systems (10).

The unidimensional, unidirection pore structure of ZSM-22 zeolites, described above, should result in good shape selective properties. These high silica zeolites have low to moderate acidities and should act as good isomerization catalysts. In modeling experiments strong evidence suggests that 10-T-ring systems are necessary for high performing butene isomerization catalysts (5). Indeed, the results of our experiments show that the shape-selective properties and low acidity of these types of materials make ZSM-22 zeolites effective catalysts for the isomerization of butenes.

Flow analyses, shown in Fig. 5, suggest that a diffusion limited region exists throughout the entire range of flow rates studied (3.5 to 100 cm^3/min). A continuous rise in the activity of these catalysts as a function of flow rate suggests that limitations due to diffusion are apparent. Under normal conditions, diffusion limited zeolitic processes occur only at very low flow rates. Typically these diffusional effects are likely to be found in deep bed reactors where intercrystalline diffusion or external diffusion is a serious concern. In our analyses, a bed depth of 1–2 cm was used; however, even at high flow rates limitations of diffusion are apparent. In earlier work with B-ZSM-11 zeolites, external diffusion is observed only up to 18 cm^3/min using comparable particle sizes and bed depths (19). One might expect the two-dimensional channel system and larger void volumes to lessen the effects of internal diffusion in B-ZSM-11 over ZSM-22; however, the phenomenon observed here appears to be a result of external diffusion only.

Complete calcination of these materials at 550°C in 20% O_2 is very difficult to achieve. Small amounts of template remained in these materials after the calcination process. This suggests that intracrystalline diffusion effects within the zeolite may inhibit the calcination processes in these systems.

The data of Table 1 show that the highest yields and selectivities to isobutylene are obtained at a temperature of 420°C. The data show that actual yields are closest to theoretical maximum yields between 420 and 460°C. At temperatures greater than 460°C the experimental yields fall well below maximum theoretical yields. At temperatures below 420°C, deviation between actual and calculated maximum yields is the greatest. This is because at lower temperatures the thermodynamic equilibrium of i-C_4H_8 is increasingly favored over n-C_4H_8 and the overall activity of the catalyst is relatively low. At temperatures greater than 480°C severe cracking reactions occur leading to rapid deactivation of the catalyst. At increasing temperatures, the thermodynamic equilibrium becomes less favorable for i-C_4H_8.

Deactivation studies suggest that the lifetime of the catalyst is optimized at 420°C. Maximum experimental yields are also obtained at this temperature with high selectivity. The operating temperature for the transformation of 1-butene to isobutylene over ZSM-22 zeolites is much lower than that of the B-ZSM-11 system which required an operating temperature of 523°C (19).

Reduced acidity pentasil zeolites produced only 28% yields of i-C_4H_8 under optimal conditions and at 523°C. In these systems, oligomer formation and catalyst deactivation were serious problems, decreasing the lifetime of the catalyst, reducing product selectivity to isobutylene, and increasing the yields of propylene (a product of cracked oligomers). The oligomerization reaction using ZSM-22 zeolites is significantly reduced. Under optimal conditions and at steady state, gas phase oligomers are reduced to less than 1%. This suggests that the presence of pore void volumes in ZSM-11 zeolites, a result of intersecting channels (5.3 × 5.5 Å and 5.4 × 5.6 Å), is a likely factor in the enhancement of oligomer formation. As mentioned earlier, ZSM-11 and ZSM-22 zeolites are expected to have similar acidities, thus suggesting that differences in shape-selectivity properties between the two systems are contributing factors in product distributions, selectivities, and oligomer formation.

The data of Fig. 6 clearly show that there is rapid deactivation within the first 5 h time on stream and a slow continuous deactivation until near steady state conditions are reached after 18 h time on stream. Increased oligomer or coke accumulation on the catalyst with increasing time on stream suggests that decreased pore volumes and/or

poisoning of strong acid sites might explain the increase in the yields of isobutylene. In the [B]-ZSM-11 system, a proposed mechanism is given suggesting that there are two different sites present on the catalyst, and that one of these sites is responsible for oligomerization (19). However, in these analyses the data suggest that transition state shape selectivity is the dominating factor.

The data of Fig. 7 show that increasing time on stream results in a decrease in lower olefins, particularly propylene, which is shown to be the major by-product of this reaction. This deactivation trend, which shows a decrease in cracking, is further evidence that acid sites are being irreversibly poisoned. Cracking is a typical acid catalytic process. Increased coke formation leads to a decrease in dimerization reactions. Coking also decreases pore size and prevents dimerization by limiting space surrounding the active sites. This is likely to contribute heavily to increased yields and selectivity to isobutylene by diminishing pore size and enhancing the shape-selective properties of the catalyst. These experiments are forthcoming in another work.

The most significant data can be found in Fig. 8. These data cleary show that the yields of isobutylene (and selectivities) are optimized at a conversion of 47%. Above this conversion the yield of C_3H_6 begins to dominate. Yields of isobutylene are heavily dependent on extent of reaction. A similar relationship between conversion and yield was observed using ferrierite-type zeolites; however, the activity of these catalysts is generally higher and low conversions were unreachable (24).

Data of Fig. 9 suggest that the isomerization reaction to isobutylene is first order in 1-butene. This is consistent with earlier work for the same reaction (19).

Regeneration of spent catalysts in 10% O_2 at 550°C show that activity can be restored to original levels. Regeneration in O_2 was more effective than in H_2. In other studies with ferrierite zeolites (25) surface areas decreased from 360 m^2/g for the freshly calcined sample to 28 m^2/g following 18 h of reaction with 20% 1-C_4H_8 at 420°C. Regeneration of the catalyst in 10% O_2 resulted in restoration of 95% of the original surface area of the material, and original catalytic activity was obtained.

V. CONCLUSIONS

ZSM-22 zeolites having the Theta-1 structure and a Si/Al ratio of 45 were synthesized using 1,6-diaminohexane as a template. X-ray powder diffraction patterns, TEM electron diffraction lines of bulk sample, and electron dot patterns of single crystals reveal that this zeolite belongs to the Theta-1 crystal type. Morphology and crystal sizes also confirm the ZSM-22 structure. Acidity measurements show that acid sites of two different strengths in nearly equal proportions are present in this material with mostly Brønsted acidity. This material has low acidity and a relatively low surface area compared to other zeolites, a result of low void volumes in the framework structure of these systems. Catalytic experiments show that ZSM-22 zeolites are effective catalysts for the isomerization of 1-butene. At 420°C, maximum isobutylene yields of 39.5% were obtained. This yield of i-C_4H_8 is the highest thermodynamically possible. Temperatures less than 420°C and greater than 460°C resulted in a large deviation between theoretical values for maximum i-C_4H_8 yields (based on thermodynamic equilibrium calculations) and experimental values. Maximum yields of i-C_4H_8 were obtained at a conversion level of 47% in this first order reaction. Increasing time on stream resulted in higher yields of isobutylene and decreased oligomer formation at low WHSV, likely due to a decrease in pore size of the zeolite, which enhances shape-selective properties. Deactivation of ZSM-22 zeolite is fast during the first 5 h and slow deactivation continues to occur until steady state is reached after 18 h. Propylene is the major by-product of the isomerization reaction. This results from the cracking of higher hydrocarbons formed during the oligomerization side reaction, presumably on the strong acid sites.

Low channel void volumes and the 10-T-ring system give Theta-1-type zeolites good shape-selective properties. Low acidity provides an excellent surface medium for mild isomerization reactions, increasing selectivities and minimizing the more severe cracking reactions.

ACKNOWLEDGMENTS

We thank Dr. Suresh K. Gupta for assistance with surface area measurements, Mr. Wen-Qing Xu for TPD results, and Mr. Larry McCurdy for TEM analysis. The authors also gratefully acknowledge Texaco, Inc., and the Department of Energy, Office of Basic Energy Sciences, Division of Chemical Sciences for support of this research.

REFERENCES

1. Weissermel, K., and Arpe, H. J., "Industrial Organic Chemistry: Important Raw Materials and Intermediates," pp. 63–68. VCH, New York, 1978.
2. *Chem. Eng. News* **70**(10), 27 (1992).
3. Kokotailo, G. T., Schlenker, J. L., Dwyer, F. G., and Valyocsik, E. W., *Zeolites* **5**, 349 (1985).
4. Marler, B., *Zeolites* **7**, 393 (1987).
5. Thomas, J. M., *Sci. Am.*, April, 112 (1992).
6. Barri, S. A., Smith, G. W., White, D., and Young, D., *Nature* **312**, 533 (1984).
7. Borade, R. B., Adnot, A., and Kaliaguine, S., *Zeolites* **11**, 710 (1991).
8. Kozo, T., and Noboru, Eur. Pat. Appl. 170,003 (1986).
9. Takatsu, K., and Kawata, N., Eur. Pat. Appl. 0087017 (1983).
10. Parker, L. M., and Bibby, D. M., *Zeolites* **3**, 8 (1983).
11. Araya, A., and Lowe, B. M., *Zeolites* **4**, 280 (1984).

12. Hogan, P. J., Stewart, A., and Whittam, T. V., E. Patent A-065,400 (1982).
13. Chang, C. D., Lang, W. H., and Bell, W. K., "Catalysis of Organic Synthesis" (W. R. Moser, Ed.), New York, Dekker (1981).
14. Spencer, M. S., and Whittam, T. V., *Acta Phys. Chem.* **24**(1–2), 307 (1978).
15. Olson, D. H., Calvert, R. B., and Valyocsik, E. W., E. Patent A-102,716 (1983).
16. Hogan, P. J., Whittam, T. V., Birtill, J. J., and Stewart, A., *Zeolites* **4,** 275 (1984).
17. Ashton, A. G., Barri, S. A. I., and Dwyer, J., *Acta Phys. Chem. Szeged.*, 25 (1985).
18. Dwyer, F. G., U. S. Patent 4,556,477 (1985).
19. Bianchi, D., Simon, M. W., Nam, S. S., Xu, W-Q., Suib, S. L., and O'Young, C-L., *J. Catal.* **145,** 551 (1994).
20. Ernst, S., Weitkamp, J., Martens, J. A., and Jacobs, P. A., *Appl. Catal.* **48,** 137 (1989).
21. Simon, M. W., Efsthathiou, A. M., Bennett, C. O., and Suib, S. L., *J. Catal.* **138,** 1 (1992).
22. Xu, W.-Q., Suib, S. L., submitted for publication (1993).
23. Simon, M. W., Nam, S. S., Xu, W.-Q., Suib, S. L., Edwards, J. C., and O'Young, C.-L., *J. Phys. Chem.* **96,** 6381 (1992).
24. Simon, M. W., Suib, S. L., and O'Young, C.-L., in preparation.
25. Simon, M. W., and Gupta, S., unpublished results.